Geophysical Research Letters

RESEARCH LETTER
10.1029/2020GL088295

Reappraisal of the Climate Impacts of Ozone-Depleting Substances

Olaf Morgenstern[1], Fiona M. O'Connor[2], Ben T. Johnson[2], Guang Zeng[1], Jane P. Mulcahy[2], Jonny Williams[1], João Teixeira[2], Martine Michou[3], Pierre Nabat[3], Larry W. Horowitz[4], Vaishali Naik[4], Lori T. Sentman[4], Makoto Deushi[5], Susanne E. Bauer[6,7], Kostas Tsigaridis[6,7], Drew T. Shindell[8], and Douglas E. Kinnison[9]

[1]National Institute of Water and Atmospheric Research (NIWA), Wellington, New Zealand, [2]Hadley Centre, Met Office, Exeter, UK, [3]Centre National de Recherches Météorologiques (CNRM), Université de Toulouse, Météo-France, CNRS, Toulouse, France, [4]Geophysical Fluid Dynamics Laboratory (GFDL), National Oceanic and Atmospheric Administration, Princeton, NJ, USA, [5]Meteorological Research Institute (MRI), Tsukuba, Japan, [6]NASA Goddard Institute for Space Studies (GISS), New York, NY, USA, [7]Center for Climate Systems Research, Columbia University, New York, NY, USA, [8]Earth and Ocean Sciences, Duke University, Durham, NC, USA, [9]National Center for Atmospheric Research (NCAR), Boulder, CO, USA

Abstract We assess the effective radiative forcing due to ozone-depleting substances using models participating in the Aerosols and Chemistry and Radiative Forcing Model Intercomparison Projects (AerChemMIP, RFMIP). A large intermodel spread in this globally averaged quantity necessitates an "emergent constraint" approach whereby we link the radiative forcing to ozone declines measured and simulated during 1979–2000, excluding two volcanically perturbed periods. During this period, ozone-depleting substances were increasing, and several merged satellite-based climatologies document the ensuing decline of total-column ozone. Using these analyses, we find an effective radiative forcing of −0.05 to 0.13 W m^{-2}. Our best estimate (0.04 W m^{-2}) is on the edge of the "likely" range given by the Fifth Assessment Report of IPCC of 0.03 to 0.33 W m^{-2} but is in better agreement with two other literature results.

Plain Language Summary Chloroflourocarbons and other compounds involved in ozone depletion are also powerful greenhouse gases, but their contribution to global warming is reduced due to the cooling effect of the ozone loss which they induce. Models informing an upcoming climate report disagree on the ozone loss and thus on the climate influence of these gases. Here we use observed ozone loss to reduce the resultant uncertainty in their overall climate influence and infer a smaller warming influence of these substances than was considered likely in a 2013 climate report. The result implies a smaller benefit to climate due to their phase-out, mandated under the Montreal Protocol, than would have been the case under previous understanding.

Key Points:
- Effective radiative forcing of ozone-depleting substances, as discerned from CMIP6 simulations, spans a large range
- Using an emergent constraint approach, our new estimate is consistent with observational climatologies of total-column ozone
- This range implies a smaller forcing than the estimate provided by the Fifth Assessment Report of the Intergovernmental Panel on Climate Change

Supporting Information:
- Supporting Information S1

Correspondence to:
O. Morgenstern,
olaf.morgenstern@niwa.co.nz

Citation:
Morgenstern, O., O'Connor, F. M., Johnson, B. T., Zeng, G., Mulcahy, J. P., Williams, J., et al. (2020). Reappraisal of the climate impacts of ozone-depleting substances. *Geophysical Research Letters*, *47*, e2020GL088295. https://doi.org/10.1029/2020GL088295

Received 7 APR 2020
Accepted 18 SEP 2020
Accepted article online 28 SEP 2020

1. Introduction

The Antarctic ozone hole remains arguably the most spectacular demonstration of human interference with the climate system. Within a few decades of starting to use chloro-fluorocarbons (CFCs) and other halocarbons on an industrial scale, humans had thinned the ozone layer above Antarctica in spring to a fraction of its prior thickness (World Meteorological Organization (WMO), 2018). This ozone depletion has had a substantial impact on the climate of the Southern Hemisphere (Banerjee et al., 2020; Goyal et al., 2019; Iglesias-Suarez et al., 2016; Kang et al., 2011; Myhre et al., 2013; Shindell et al., 2013; Thompson et al., 2011). In 1987 the Montreal Protocol was enacted and subsequently strengthened which mandates a phase-out of these ozone-depleting substances (ODSs). It has been hailed as the most successful international treaty ever to protect the environment (Prather et al., 1996). Several of these ODSs (particularly the leading CFCs, CFC-11 and CFC-12) also act as greenhouse gases, with global warming potentials many thousands of times larger than that of CO_2 (table 8.A.1 of Myhre et al., 2013; World Meteorological Organization (WMO), 2018). By phasing them out, the Montreal Protocol is thought to have averted more global warming than the Kyoto Protocol (Velders et al., 2007). The Fifth Assessment Report of IPCC (AR5; Myhre et al., 2013) estimates that in 2011 ODSs regulated by the Montreal Protocol exerted a direct radiative forcing of 0.34 W m^{-2} and a net radiative forcing, accounting for ozone depletion, of 0.18 ± 0.15 W m^{-2} relative to preindustrial times.

Table 1
Models, key References, and "Historical" and "Hist-1950HC" Simulations Denoted by their Run Numbers

Model name	Reference	Historical sims.	Hist-1950HC sims.
CESM2-WACCM	Gettelman et al. (2019)	1, 2, 3	1
CNRM-ESM2-1	Séférian et al. (2019)	1 to 5, 8, 9, 10	2, 3
GFDL-ESM4	Dunne et al. (2020)	1	1
GISS-E2-1-G	Kelley et al. (2020)	6, 8, 9, 10	1
MRI-ESM2-0	Yukimoto et al. (2019)	1 to 5	1, 2, 3
UKESM1-0-LL	Sellar et al. (2019)	1 to 4, 8 to 12, 16 to 19	1

Accordingly, AR5 assesses that ODSs "very likely" have a positive radiative forcing as their direct radiative effects outweigh the indirect impact of ozone depletion. AR5 postulates a reduced RF of ozone depletion versus Søvde et al. (2011) and Shindell et al. (2013) because both studies find larger absolute radiative forcing of ozone depletion than the mean of a multimodel experiment (p. 679 of Myhre et al., 2013), which however also underestimates springtime ozone loss, particularly in the Arctic (Iglesias-Suarez et al., 2016).

AR5 thus finds a large uncertainty associated with the radiative forcing offset due to ozone depletion. Furthermore, AR5 uses the "stratospherically adjusted radiative forcing" concept, whereby any atmospheric adjustments other than a temperature adjustment of the stratosphere are not considered. AR5 considers these minor effects. These issues motivate a reassessment using new models and methodologies. AerChemMIP and RFMIP (Collins et al., 2017; Pincus et al., 2016) are coordinated efforts to reassess these radiative forcing processes using newer models and taking into account all atmospheric adjustments, arriving at the "effective radiative forcing" (ERF; Forster et al., 2016). In particular, here we will use simulations submitted under the "piClim-control" and the "piClim-HC" experiments. Both are atmosphere-only simulations driven with preindustrial sea surface conditions and all atmospheric forcings at preindustrial levels, except that in the case of piClim-HC surface abundances of halogenated ODS compounds (short: halocarbons, HCs) are elevated to their 2014 mean surface volume mixing ratios (Meinshausen et al., 2017). The difference in the global, multiannual mean net top-of-the-atmosphere radiation between this pair of simulations defines the ERF due to ODSs. The problem, detailed below, is that this approach yields large intermodel differences for this ERF. A technique to deal with such model disparities is known as an "emergent constraint" (EC; e.g., Williamson & Sansom, 2019). This consists of relating a theoretical concept (such as the ERF of ODSs) to a different, physically related quantity, which good-quality historical observational data exist for. To constrain the ERF of ODSs, we evaluate here the choice of total-column ozone (TCO) measured comprehensively by satellite, airborne, and ground-based instruments since the latter decades of the 20th century when ODSs were sharply increasing over time and ozone depletion was established. These measurements are here compared directly to allforcings "historical" simulations produced for CMIP6. We also use TCO and vertically resolved ozone fields from the "hist-1950HC" simulations, which differ from the "historical" ones in that ODSs are held constant at their 1950s abundances. The remainder of this paper is devoted to applying this approach to AerChemMIP/RFMIP and "historical" (Eyring et al., 2016) simulations to arrive at a recommended value for the ERF of ODSs.

2. Method, Models, and Observational Data

We use here six different climate models, listed in Table 1.

We choose these models because (a) all of them include explicit stratospheric chemistry and (b) required data from these models are available for the piClim-control, piClim-HC, historical, and hist-1950HC experiments. Here we use total-column and vertically resolved ozone, temperature (needed to derive ozone concentrations), and outgoing shortwave and longwave radiation at the top of the atmosphere, all in monthly means. The piClim-control and piClim-HC experiments all are one-member-per-model ensembles; the last 20 years of these simulations are used. We have established that the halocarbon increase in the piClim-HC simulation versus piClim-control has been fully communicated to the ozone layer and the ensuing ozone depletion is fully realized (Figure S1 in the supporting information).

Table 2
Three Observational TCO Climatologies and the Reference Ozone Field Used to Force CMIP6 Models Without Interactive Ozone

Data set	Coverage	Resolution	Reference
TOMS-SBUV v8	1978–2005	Zonal mean, 5°	Frith et al. (2014)
NIWA-BS (v3.4, unpatched)	1978–2016	1° × 1°	Bodeker et al. (2005)
MSR-2	1979–2018	0.5° × 0.5°	van der A et al. (2015)
CMIP6	1850–2014	2.5° × 1.5°	Checa-Garcia et al. (2018)

The "historical" simulations include all forcings and thus are directly comparable to four different ozone climatologies listed in Table 2. Here we only consider data from the period 1979–2000 when ozone depletion was established. Three of these data sets are based on satellite measurements but may use different versions and/or combine them in different ways with ground-based and airborne/balloon measurements to account for offsets between different overlapping satellite time series, data gaps, drifts, and other instrumental artifacts. Details are in the references given (Table 2). Furthermore, we consider TCO derived from the ozone forcing data set (Checa-Garcia et al., 2018) recommended to be used by CMIP6 models that do not compute their own ozone. Referred to here as "CMIP6", this is not an observational data set; rather, it is derived from two "historical" chemistry-climate model simulations. In all TCO data sets we remove two years each after the major volcanic eruptions of El Chichón (March 1982) and Mt. Pinatubo (June 1991) although retaining these data would only have a small influence on our results. For consistency, all model and observational data sets are processed to form zonal means on a common 0.5° latitude grid with identical data gaps restricted to the polar nights (this is expanded in the supporting information).

The EC technique relies on a linear regression relating TCO trends averaged globally or regionally to simulated ERF averaged over the same regions. Both the TCO trends and the ERF estimates are subject to statistical uncertainties. (These are expressed throughout this paper for a 68% or one standard-deviation confidence level. This is similar to the "likely" range in the IPCC's calibrated uncertainty language; Mastrandrea et al., 2011.) Furthermore, there are some differences between the observational climatologies. We use a Monte Carlo (random perturbation) technique to quantify how these uncertainties project onto our best estimate for the ERF. This is expanded upon more in section S2.

3. Ozone Trends and the Suitability of TCO for Constraining the ERF of ODSs

We calculate trends in zonal-mean TCO for the period 1979–2000 for the four reference data set and the six models (Figures 1, S2, and S4) excluding 2 years each after El Chichón and Mt. Pinatubo. There are mostly relatively small differences between the observational data sets, as expected. The CMIP6 ozone climatology compares well with the observations in the Southern Hemisphere but underestimates the decline in Northern Hemisphere ozone.

The six climate models exhibit highly variable Antarctic ozone trends in their ensemble-average historical simulations (Figure 1), ranging from quite weak (MRI-ESM2-0) to extremely strong (GISS-E2-1-G). In the Arctic, several models (CESM2-WACCM, GFDL-ESM4, and MRI-ESM2-0) exhibit weak trends, whereas UKESM1 and GISS-E2-1-G exhibit excessive ozone depletion in both polar regions.

For the EC analysis to be valid, differences in TCO trends between the models need to be predominantly driven by differences in their responses to ODSs. Considerations here include that at least in models, and likely in reality, some reductions in stratospheric ozone occurred before the onset of comprehensive satellite measurements in 1978 (Figure S4; Dhomse et al., 2018); that the actual ozone depletion occurred in an atmosphere with the methane loading increased above its preindustrial level, which reduces the efficiency of chlorine at depleting ozone; and that stratospheric cooling since preindustrial times due to increasing greenhouse gases (GHGs) affects both polar and extrapolar ozone chemistry in different ways (Morgenstern et al., 2018). Single-forcing model simulations consistently show that the net effect of these GHGs increasing during the ozone-depletion period has been to mitigate some ozone depletion (Dhomse et al., 2018; Eyring et al., 2010).

A comparison of ozone simulated in "historical" versus hist-1950HC experiments indicates that trends associated with ODSs during 1979–2000 are substantially larger than those associated with other influences (Figures 1, S2, and S3). The hist-1950HC simulations reveal some increases in TCO (which are always

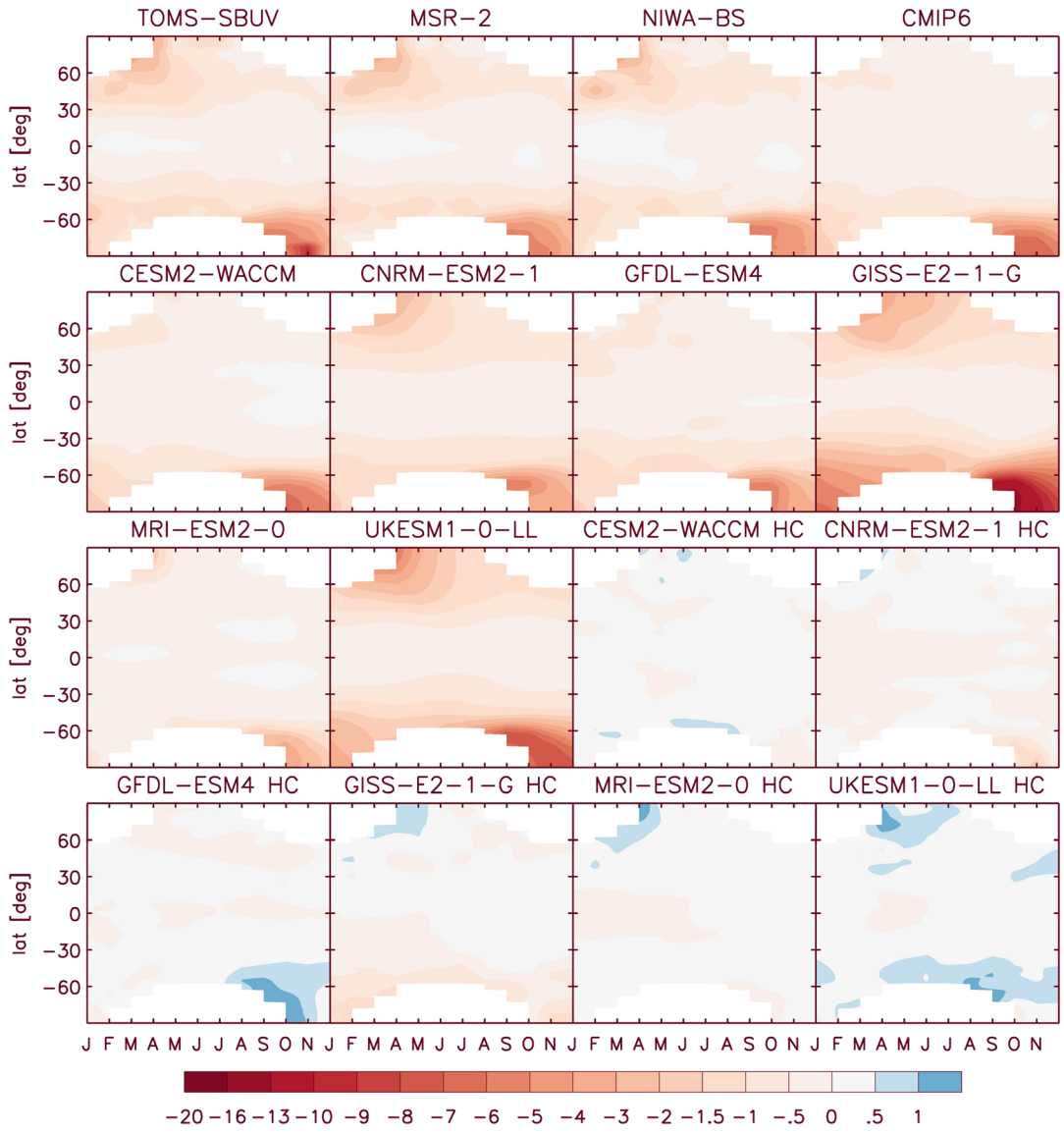

Figure 1. Zonal-mean TCO trends (Dobson units/year, DU a^{-1}) for 1979–2000, excluding two years each after the El Chichón and Pinatubo eruptions, in three observational data sets (TOMS-SBUV, NIWA-BS, and MSR-2), the CMIP6 ozone climatology, and the ensemble-average "historical" and "hist-1950HC" simulations (marked "HC") by the six CMIP6 models considered here. White regions denote polar-winter data gaps.

smaller than about 2 DU a^{-1}), but also decreases, particularly in the Southern Hemisphere in the case of the GISS-E2-1-G model (Figure 1). This will be further elaborated upon below. Vertically resolved trends show that these trends have contributions both due to some tropospheric ozone increases (which in all cases are much smaller than the stratospheric decreases due to ODSs), but also decreases and increases in the stratosphere in the hist-1950HC simulations that are presumably the result of increasing GHGs during the study period (Figure S3; Morgenstern et al., 2018). ODSs impose a consistent signal on the simulations of ozone, with losses in all models peaking at 70 hPa. The large variations in the amplitude of this ozone loss are reflected in corresponding intermodel differences in the TCO trends noted above (Figures 1 and S3).

4. The Emergent-Constraint analysis

We perform a formal pattern similarity analysis on the TCO differences and trends shown in Figures 1 and S5 (Figure 2). Five models cluster at a pattern correlation exceeding 0.94 and a trend to difference ratio of

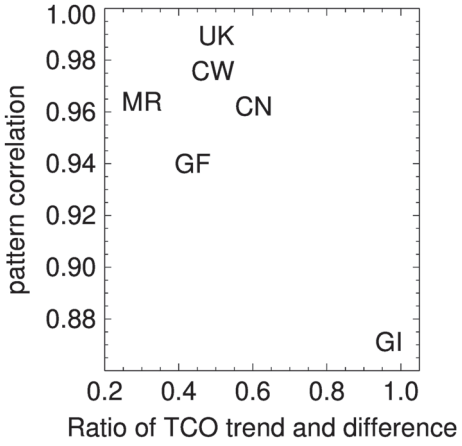

Figure 2. Abscissa: ratio of area-weighted, global- and annual-mean ozone trend (DU a^{-1}) for 1979–2000 derived from the historical simulations, with two volcanically perturbed periods removed (Figure 1), and the global- and annual-mean ozone difference (DU) between the piClim-HC and piClim-control experiments (Figure S1) divided by 22 years. Ordinate: pattern correlation between the zonal-mean ozone trends shown in Figure 1 and the zonal-mean ozone differences between the piClim-HC and piClim-control experiments, for the six CMIP6 models (Figure S5). CN = CNRM-ESM2-1; CW = CESM2-WACCM; GF = GFDL-ESM4; GI = GISS-E2-1-G; MR = MRI-ESM2-0; UK = UKESM1-0-LL.

around 0.3 to 0.6 (i.e., the global ozone loss deduced from historical simulations between 1979 and 2000 is 30% to 60% of the difference in ozone between the piClim-control and piClim-HC simulations). GISS-E2-1-G has a somewhat lower correlation but a much larger trend ratio. This model exhibits a much bigger response to volcanic eruptions than the other models (e.g., after the Krakatoa eruption of 1883) and enters into a volcanically disturbed phase of increased TCO in the 1970s (Figure S4). This implies that in this model, the 1979–2000 trend has a substantial contribution due to recovery from this volcanic perturbation (which may also cause the Southern Hemisphere ozone loss in the hist-1950HC simulation by this model; Figure 1). This manifests as an anomalous amplification of the influence of ODSs as the volcanic effect transitions from increasing TCO under low chlorine conditions to decreasing it during times of high chlorine loading. For this reason GISS-E2-1-G is not considered in the EC analysis. Since its piClim-control and piClim-HC simulations are not affected by this problem, we do report the ERF of ODSs derived from these GISS-E2-1-G simulations (Table 3). The GISS-E2-R model used by Shindell et al. (2013) does not have this problem and should not be assumed to behave similarly to GISS-E2-1-G.

The ERF of ODSs closely relates to how much ozone depletion is simulated in the five models, which is the basis for our EC analysis (Figure 3). We capture this relationship through a least-squares linear regression line. Where this line intersects with the ozone depletion discerned from the average of the three observational climatologies defines the ERF of ODSs that optimally corresponds to observed ozone loss. One standard-deviation error bounds in this analysis are the result of a Monte Carlo simulation detailed in the supporting information. Table 3 summarizes the ERFs discerned in this way. A comparison with the straightforward multimodel mean (MMM) reveals that these analyses lead to a considerable reduction of the uncertainty. A caveat in both cases is that the uncertainty analysis presented here is purely statistical in nature and does not fully capture some aspects of the total uncertainty such as sampling uncertainty (caused by the small number of models considered here) and model uncertainty (caused by structural and formulation problems which may be common to different models).

Table 3
ERFs of ODSs (W m^{-2})

Climatology	90°S to 90°N	0° to 90°N	90°S to 0°	60°S to 60°N
CESM2-WACCM	0.31 ± 0.09	0.43 ± 0.10	0.19 ± 0.13	0.41 ± 0.11
CNRM-ESM2-1	-0.19 ± 0.04	0.00 ± 0.05	-0.38 ± 0.06	-0.09 ± 0.05
GFDL-ESM4	0.06 ± 0.04	0.19 ± 0.05	-0.07 ± 0.06	0.16 ± 0.05
GISS-E2-1-G	0.28 ± 0.05	0.23 ± 0.05	0.33 ± 0.05	0.38 ± 0.05
MRI-ESM2-0	0.30 ± 0.07	0.40 ± 0.09	0.20 ± 0.08	0.34 ± 0.08
UKESM1-0-LL	-0.16 ± 0.05	0.06 ± 0.07	-0.37 ± 0.06	0.00 ± 0.06
MMM	0.10 ± 0.24	0.22 ± 0.19	-0.17 ± 0.31	0.20 ± 0.22
MSR-2	0.05 ± 0.08	0.16 ± 0.08	-0.05 ± 0.10	0.14 ± 0.08
NIWA-BS	0.07 ± 0.07	0.17 ± 0.07	-0.02 ± 0.10	0.17 ± 0.08
TOMS-SBUV	-0.01 ± 0.09	0.13 ± 0.09	-0.13 ± 0.11	0.09 ± 0.10
MOM	0.04 ± 0.09	0.15 ± 0.09	-0.07 ± 0.11	0.13 ± 0.10
Prob. of neg. value	24%	4%	56%	5%
CMIP6	0.15 ± 0.08	0.33 ± 0.07	-0.06 ± 0.10	0.24 ± 0.08
Søvde et al. (2011)	0.08			
Shindell et al. (2013)	0.13 ± 0.07			
Myhre et al. (2013)	0.18 ± 0.15			

Note. Model results and multimodel mean (MMM) with their respective errors at 68% confidence (1σ). Derived ERFs for the three ozone climatologies and their "multi-observations mean" (MOM), and the CMIP6 climatology. These ERFs are evaluated using the EC technique. For the MOM we state the probability of this value being negative. For reference we also include three literature values discussed in the main text. Radiative-forcing values by Søvde et al. (2011) and Shindell et al. (2013) are adjusted assuming a direct radiative forcing of due to ODSs of 0.34 W m^{-2} (Myhre et al., 2013).

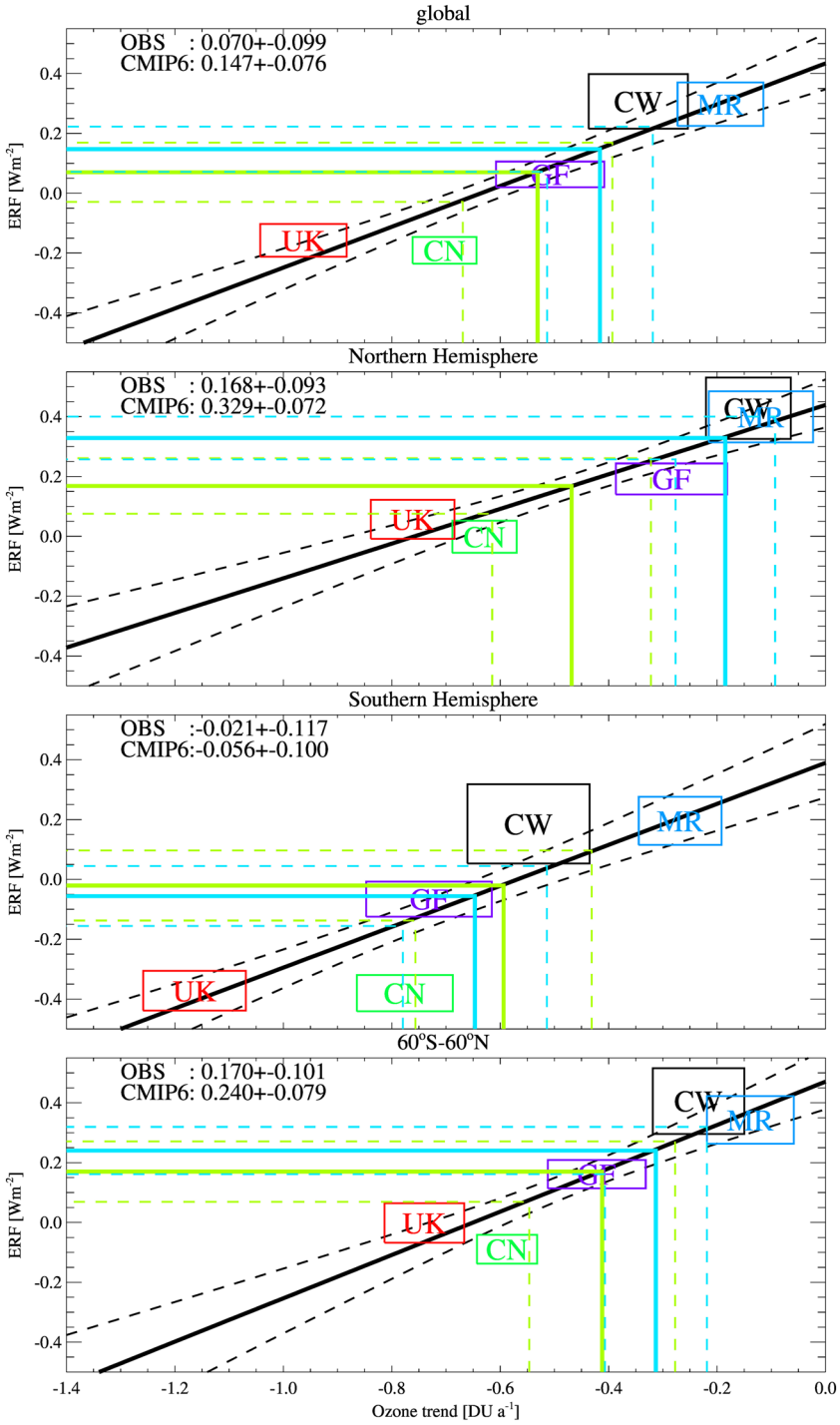

Figure 3. Colored rectangles: area-mean ozone trend for 1979–2000 and ERF of ODSs (accounting for all feedbacks) simulated by the five CMIP6 models. The width and height of the rectangles represent the statistical uncertainties of these quantities at the one-standard deviation or 68% confidence level. Black lines: least-squares linear fit (solid) with associated 68% confidence uncertainties (dashed). Green lines: estimated observational ozone depletion (solid) with its 68% confidence uncertainty (dashed) derived from the NIWA-BS climatology, and the corresponding projection onto the ERF of ODSs. Light blue lines: the same but for the CMIP6 ozone climatology. The four panels represent the global, Northern-Hemisphere, Southern-Hemisphere, and 60°S to 60°N means for ozone depletion and the ERF. The labels in the top left corners of the panels represent the ERF of ODSs in W m^{-2} consistent with the EC calculation for the observations ("OBS") and the CMIP6 climatology ("CMIP6"). CN = CNRM-ESM2-1; CW = CESM2-WACCM; GF = GFDL-ESM4; MR = MRI-ESM2-0; UK = UKESM1-0-LL. Note that the inflection points for the uncertainty bounds (dashed green and blue lines) are located slightly off the EC (thick black line), a result of combining the uncertainty in ozone depletion with that in the EC.

5. Discussion and Conclusions

The present state-of-understanding regarding the radiative forcing of ODSs is that in the global average their combined direct heat-trapping properties dominate the cooling impact of ozone depletion, such that their net radiative forcing is "very likely" positive (Myhre et al., 2013). However, this assessment is inconsistent with our multimodel analysis conducted on CMIP6 simulations. We use an emergent-constraint approach to account for large biases in the simulation of ozone depletion characterizing these simulations; this approach turns these biases into assets necessary for the analysis to become robust. We find a best-estimate ERF on the edge of the range given by Myhre et al. (2013). It is associated with a "likely" uncertainty range which includes zero. This finding also provides a new perspective on an earlier conclusion that the Montreal Protocol has been of greater benefit to climate than the Kyoto Protocol (Velders et al., 2007)—while true for the direct RF of ODSs, this may not hold for the ERF of ODSs. Of course the ERF of ODSs is not the only measure of climate impact. The leading impact of ozone depletion is a well-understood summertime speed-up of southern-extratropical westerly winds and a poleward displacement of circulation regimes that the Montreal Protocol has helped arrest (e.g., Banerjee et al., 2020; Goyal et al., 2019).

In detail, our analysis has shown that historical TCO trends for 1979–2000 simulated by CMIP6 full-chemistry models, with volcanic periods ignored, correlate with the total ozone loss caused by anthropogenic ODSs simulated by the same models. This means that observed TCO loss provides the "emergent constraint" on an otherwise highly uncertain quantity. This analysis depends to some extent on the ozone depletion evident in the observational climatologies. The differences between them, though small, contribute to the uncertainty in the best-estimate ERF of ODSs. Relative to the average of three observational climatologies, the ERF of ODSs likely falls into the range of −0.05 to 0.13 W m^{-2}; that is, there is a 24% probability that the ERF of ODSs is actually negative. (As an aside, the CFC-12 equivalent mixing ratio of ODSs only dropped by 0.4% between 2011 and 2014, meaning their direct radiative forcing is essentially unchanged during this period; Meinshausen et al., 2017).

Extrapolation of the regression line in Figure 3 to zero ozone loss yields a global-mean ERF of ODSs, thus excluding the direct and indirect impacts of ozone depletion, of 0.43 (0.35 to 0.53) W m^{-2} in all cases. This is slightly larger than (though consistent at the 95% confidence level with) the AR5 estimate for the direct radiative forcing of ODSs of 0.34 W m^{-2} (Myhre et al., 2013), possibly because of additional feedbacks not included in the AR5 calculation, but also possibly highlighting that the EC analysis conducted here is based on only five models all using low spectral-resolution radiative transfer schemes and hence is somewhat uncertain. Such additional feedbacks include cloud and aerosol effects of ozone-depleting substances briefly discussed in the supporting information. We adopt the AR5 assessment for the direct RF of ODSs (0.34 W m^{-2}) because it is based on more accurate radiative-transfer calculations than are feasible to conduct within a chemistry-climate model.

The analysis finds a negative central estimate of the total ERF of ODSs in the Southern Hemisphere of -0.07 ± 0.11 W m^{-2} (Table 3), in qualitative agreement with Shindell et al. (2013). For the Northern Hemisphere, in all cases the analysis yields positive ERFs, reflecting the lesser role of ozone depletion here. If the analysis is restricted to the latitude range 60°S to 60°N, thus excluding the polar regions, the uncertainty range is essentially the same (0.2 W m^{-2}) as if the analysis is extended to the whole globe, suggesting that the mid- and low-latitude differences between the TCO climatologies play a significant role in driving the uncertainty in the global ERF.

Turning now to the CMIP6 ozone climatology (Checa-Garcia et al., 2018), the weak Northern-Hemisphere ozone depletion in this climatology relative to observations (Figure 1) causes a larger total global-mean ERF (0.15 W m^{-2}) than would be consistent with the observations. In the Southern Hemisphere, ozone loss and thus the ERF of ODSs associated with this climatology (-0.06 ± 0.1 W m^{-2}) compare well with the observational estimates.

In summary, we find here a global-mean ERF of ODSs of 0.04 ± 0.09 W m^{-2}, which is on the edge of the "likely" range given in AR5 of 0.18 ± 0.15 W m^{-2}. The central estimate of AR5, 0.18 W m^{-2}, is outside the 68% confidence range derived here. Our finding is however consistent with two literature estimates (Shindell et al., 2013; Søvde et al., 2011).

Our findings imply that during recent decades of increasing ODSs, ozone depletion has exerted a regional cooling influence in the Southern Hemisphere—and particularly in Antarctica—which has more than compensated for the direct warming effect of ODSs. For the coming decades, projected removal of ODSs from the atmosphere assuming compliance with the Montreal Protocol (World Meteorological Organization (WMO), 2018) will provide less benefit to climate than was anticipated under previous understanding (Myhre et al., 2013) because concurrent ozone increases will counterbalance most or all of the negative direct radiative forcing associated with this removal.

Data Availability Statement

Computing and data storage resources, including the Cheyenne supercomputer (doi:10.5065/D6RX99HX), were provided by the Computational and Information Systems Laboratory (CISL) at NCAR. We thank Bodeker Scientific, funded by the DSNSC, NASA, and KNMI for providing the total-column ozone databases. Processed total-column ozone data sets and scripts needed to produce the figures and numerical results presented here are available online (at https://zenodo.org/record/3923155). Original data used in this study are all publicly available at https://acd-ext.gsfc.nasa.gov/Data_services/merged/data/additional_files/toms_sbuv.v8.mod_v3.78-05.za.rev2.txt, https://www.bodekerscientific.com/data/total-column-ozone, https://www.temis.nl/protocols/O3global.html, and the CMIP6 portals (https://esgf-node.llnl.gov/search/cmip6/ and https://esgf-node.llnl.gov/search/input4mips/).

Acknowledgments

O. M., F. O. C., B. J., G. Z., J. P. M., J. W., and J. T. acknowledge the UKESM1 team and other colleagues for their support, in particular, Luke Abraham, Paul Griffiths, Mohit Dalvi, James Manners, and Omar Jamil. O. M. and G. Z. were supported by the NZ Government's Strategic Science Investment Fund (SSIF) through the NIWA program CACV. F. O. C., B. J., and J. P. M. were supported by the Met Office Hadley Centre Climate Program funded by BEIS and Defra (Grant Number GA01101). J. W. acknowledges support by the Deep South National Science Challenge (DSNSC), funded by the New Zealand Ministry for Business, Innovation and Employment (MBIE). The authors acknowledge the contribution of NeSI high-performance computing facilities to the results of this research. New Zealand's national facilities are provided by the New Zealand eScience Infrastructure (NeSI) and funded jointly by NeSI's collaborator institutions and through MBIE's Research Infrastructure programme. M. M. and P. N. particularly acknowledge the support of the entire team in charge of the CNRM climate models, and especially that of Antoinette Alias and Laurent Franchisteguy for their technical assistance. Supercomputing time was provided by the Météo-France/DSI supercomputing center. Makoto Deushi was partly supported by JSPS KAKENHI Grant No. JP20K04070. The CESM project is supported primarily by the National Science Foundation (NSF). This material is based upon work supported by the National Center for Atmospheric Research (NCAR), which is a major facility sponsored by the NSF under Cooperative Agreement 1852977.

References

Banerjee, A., Fyfe, J. C., Polvani, L. M., Waugh, D., & Chang, K.-L. (2020). A pause in Southern Hemisphere circulation trends due to the Montreal Protocol. *Nature*, *579*, 544–548. https://doi.org/10.1038/s41586-020-2120-4

Bodeker, G. E., Shiona, H., & Eskes, H. (2005). Indicators of Antarctic ozone depletion. *Atmospheric Chemistry and Physics*, *5*, 2603–2615. https://doi.org/10.5194/acp-5-2603-2005

Checa-Garcia, R., Hegglin, M. I., Kinnison, D., Plummer, D. A., & Shine, K. P. (2018). Historical tropospheric and stratospheric ozone radiative forcing using the CMIP6 database. *Geophysical Research Letters*, *45*, 3264–3273. https://doi.org/10.1002/2017GL076770

Collins, W. J., Lamarque, J.-F., Schulz, M., Boucher, O., Eyring, V., Hegglin, M. I., et al. (2017). AerChemMIP: Quantifying the effects of chemistry and aerosols in CMIP6. *Geoscientific Model Development*, *10*(2), 585–607. https://doi.org/10.5194/gmd-10-585-2017

Dhomse, S. S., Kinnison, D., Chipperfield, M. P., Salawitch, R. J., Cionni, I., Hegglin, M. I., et al. (2018). Estimates of ozone return dates from Chemistry-Climate Model Initiative simulations. *Atmospheric Chemistry and Physics*, *18*, 8409–8438. https://doi.org/10.5194/acp-18-8409-2018

Dunne, J. P., Horowitz, L. W., Adcroft, A. J., Ginoux, P., Held, I. M., John, J. G., et al. (2020). The GFDL Earth System Model version 4.1 (GFDL-ESM4.1): Overall coupled model description and simulation characteristics. *Journal of Advances in Modeling Earth Systems*, *12*, e2019MS002015. https://doi.org/10.1029/2019MS002015

Eyring, V., Bony, S., Meehl, G. A., Senior, C. A., Stevens, B., Stouffer, R. J., & Taylor, K. E. (2016). Overview of the Coupled Model Intercomparison Project Phase 6 (CMIP6) experimental design and organization. *Geoscientific Model Development*, *9*(5), 1937–1958. https://doi.org/10.5194/gmd-9-1937-2016

Eyring, V., Cionni, I., Bodeker, G. E., Charlton-Perez, A. J., Kinnison, D. E., Scinocca, J. F., et al. (2010). Multi-model assessment of stratospheric ozone return dates and ozone recovery in CCMVal-2 models. *Atmospheric Chemistry Physics*, *10*, 9451–9472. https://doi.org/10.5194/acp-10-9451-2010

Forster, P. M., Richardson, T., Maycock, A. C., Smith, C. J., Samset, B. H., Myhre, G., et al. (2016). Recommendations for diagnosing effective radiative forcing from climate models for CMIP6. *Journal of Geophysical Research: Atmospheres*, *121*, 12,460–12,475. https://doi.org/10.1002/2016JD025320

Frith, S. M., Kramarova, N. A., Stolarski, R. S., McPeters, R. D., Bhartia, P. K., & Labow, G. J. (2014). Recent changes in total column ozone based on the SBUV Version 8.6 merged ozone data set. *Journal of Geophysical Research: Atmospheres*, *119*, 9735–9751. https://doi.org/10.1002/2014JD021889

Gettelman, A., Mills, M. J., Kinnison, D. E., Garcia, R. R., Smith, A. K., Marsh, D. R., et al. (2019). The Whole Atmosphere Community Climate Model version 6 (WACCM6). *Journal of Geophysical Research: Atmospheres*, *124*, 12,380–12,403. https://doi.org/10.1029/2019JD030943

Goyal, R., England, M. H., Gupta, A. S., & Jucker, M. (2019). Reduction in surface climate change achieved by the 1987 Montreal Protocol. *Environmental Research Letters*, *14*(12), 124041. https://doi.org/10.1088/1748-9326/ab4874/pdf

Iglesias-Suarez, F., Young, P. J., & Wild, O. (2016). Stratospheric ozone change and related climate impacts over 1850–2100 as modelled by the ACCMIP ensemble. *Atmospheric Chemistry and Physics*, *16*(1), 343–363. https://doi.org/10.5194/acp-16-343-2016

Kang, S. M., Polvani, L. M., Fyfe, J. C., & Sigmond, M. (2011). Impact of polar ozone depletion on subtropical precipitation. *Science*, *332*(6032), 951–4. https://science.sciencemag.org/content/332/6032/951

Kelley, M., Schmidt, G. A., Nazarenko, L., Bauer, S. E., Ruedy, R., Russell, G. L., et al. (2020). GISS-E2.1: Configurations and climatology. *Journal of Advances in Modelling Earth Systems*, *12*, e2019MS002025. https://doi.org/10.1029/2019MS002025

Mastrandrea, M. D., Mach, K. J., Plattner, G.-K., Edenhofer, O., Stocker, T. F., Field, C. B., et al. (2011). The IPCC AR5 guidance note on consistent treatment of uncertainties: A common approach across the working groups. *Climatic Change*, *108*, 675. https://doi.org/10.1007/s10584-011-0178-6

Meinshausen, M., Vogel, E., Nauels, A., Lorbacher, K., Meinshausen, N., Etheridge, D. M., et al. (2017). Historical greenhouse gas concentrations for climate modelling (CMIP6). *Geoscientific Model Development*, *10*, 2057–2116. https://doi.org/10.5194/gmd-10-2057-2017

Morgenstern, O., Stone, K. A., Schofield, R., Akiyoshi, H., Yamashita, Y., Kinnison, D. E., et al. (2018). Ozone sensitivity to varying greenhouse gases and ozone-depleting substances in CCMI-1 simulations. *Atmospheric Chemistry and Physics*, *18*, 1091–1114. https://doi.org/10.5194/acp-18-1091-2018

Myhre, G., Shindell, D., Bron, F.-M., Collins, W., Fuglestvedt, J., Huang, J., et al. (2013). Anthropogenic and Natural Radiative Forcing. In T. F. Stocker et al. (Eds.), *Climate Change 2013 - The Physical Science Basis. Contribution of Working Group I to the Fifth Assessment Report of the Intergovernmental Panel on Climate Change* (pp. 659–740). Cambridge, UK and New York, NY: Cambridge University Press. Retrieved from https://www.ipcc.ch/site/assets/uploads/2018/02/WG1AR5_Chapter08_FINAL.pdf

Pincus, R., Forster, P. M., & Stevens, B. (2016). The Radiative Forcing Model Intercomparison Project (RFMIP): Experimental protocol for CMIP6. *Geoscientific Model Development*, *9*, 3447–3460. https://doi.org/10.5194/gmd-9-3447-2016

Prather, M., Midgley, P., Rowland, F., & Stolarski, R. (1996). The ozone layer: The road not taken. *Nature*, *381*, 551–554. https://doi.org/10.1038/381551a0

Séférian, R., Nabat, P., Michou, M., Saint-Martin, D., Voldoire, A., Colin, J., et al. (2019). Evaluation of CNRM Earth System Model, CNRM-ESM2-1: Role of earth system processes in present-day and future climate. *Journal of Advances in Modeling Earth Systems*, *11*, 4182–4227. https://doi.org/10.1029/2019MS001791

Sellar, A. A., Jones, C. G., Mulcahy, J. P., Tang, Y., Yool, A., Wiltshire, A., et al. (2019). UKESM1: Description and evaluation of the U.K. Earth System Model. *Journal of Advances in Modeling Earth Systems*, *11*, 4513–4558. https://doi.org/10.1029/2019MS001739

Shindell, D., Faluvegi, G., Nazarenko, L., Bowman, K., Lamarque, J.-F., Voulgarakis, A., et al. (2013). Attribution of historical ozone forcing to anthropogenic emissions. *Nature Climate Change*, *3*, 567. Retrieved from https://www.nature.com/articles/nclimate1835

Søvde, O. A., Hoyle, C. R., Myhre, G., & Isaksen, I. S. A. (2011). The HNO_3 forming branch of the HO_2 + NO reaction: Pre-industrial-to-present trends in atmospheric species and radiative forcings. *Atmospheric Chemistry and Physics*, *11*, 8929–8943. https://doi.org/10.5194/acp-11-8929-2011

Thompson, D., Solomon, S., Kushner, P., England, M. H., Grise, K. M., & Karoly, D. J. (2011). Signatures of the Antarctic ozone hole in Southern Hemisphere surface climate change. *Nature Geoscience*, *4*, 741–749. https://doi.org/10.1038/ngeo1296

van der A, R. J., Allaart, M. A. F., & Eskes, H. J. (2015). Extended and refined multi sensor reanalysis of total ozone for the period 1970–2012. *Atmospheric Measurement Techniques*, *8*, 3021–3035. https://doi.org/10.5194/amt-8-3021-2015

Velders, G. J. M., Andersen, S. O., Daniel, J. S., Fahey, D. W., & McFarland, M. (2007). The importance of the Montreal Protocol in protecting climate. *Proceedings of the National Academy of Sciences*, *104*, 4814–4819. Retrieved from https://www.pnas.org/content/104/12/4814.abstract

World Meteorological Organization (WMO) (2018). *Scientific Assessment of Ozone Depletion: 2018*, *Global Ozone Research and Monitoring Project* (Report No. 58, 588 pp.). Geneva, Switzerland.

Williamson, D. B., & Sansom, P. G. (2019). How are emergent constraints quantifying uncertainty and what do they leave behind? *Bulletin of the American Meteorological Society*, *100*(12), 2571–2588. https://doi.org/10.1175/BAMS-D-19-0131.1

Yukimoto, S., Kawai, H., Koshiro, T., Oshima, N., Yoshida, K., Urakawa, S., et al. (2019). The Meteorological Research Institute Earth System Model Version 2.0, MRI-ESM2.0: Description and basic evaluation of the physical component. *Journal of the Meteorological Society of Japan Ser. II*, *97*(5), 931–965. https://doi.org/10.2151/jmsj.2019-051